Fast and accurate selection of surfactants for enhanced oil recovery by dynamic Salinity-Phase-Inversion (SPI)

Guillaume Lemahieu, Jesús F. Ontiveros, Nathaniel Terra Telles Souza, Valérie Molinier, Jean-Marie Aubry

Fast and accurate selection of surfactants for Enhanced Oil Recovery by Dynamic Salinity-Phase-Inversion (SPI)

Guillaume Lemahieu[1], Jesús Fermin Ontiveros[1], Nathaniel Terra Telles Souza[2], Valérie Molinier[2*], Jean-Marie Aubry[1*]

(1) Univ. Lille, CNRS, Centrale Lille, ENSCL, Univ. Artois, UMR 8181– UCCS – Unité de Catalyse et Chimie du Solide, F-59000 Lille, France, jean-marie.aubry@univ-lille.fr

(2) Total Exploration Production, Pôle d'Etudes et de Recherche de Lacq, B.P. 47, 64170 Lacq, France, valerie.molinier@total.com

Abstract

In conventional chemical Enhanced Oil Recovery (EOR), surfactant mixtures must be optimized to obtain the so-called "optimum formulation" characterized by a three-phase behaviour (WIII) and an ultra-low interfacial tension between crude oil and injected water. To attain this condition, discontinuous salinity scans of Surfactant-Oil-Water (SOW) systems are usually performed in a series of sealed pipettes maintained at the reservoir temperature until complete phase separation. Furthermore, some SOW mixtures do not give a WIII, but instead they form viscous phases which are very detrimental for EOR applications.

The study herein describes a novel method called dynamic Salinity-Phase-Inversion (SPI) to quickly and accurately determine the optimum formulation and to anticipate whether the surfactant mixture will provide, by the conventional static method, a WIII or a viscous phase. This method consists in continuously modifying the salinity of a stirred SOW system at WOR in the vicinity of 1, in order to detect the phase inversion of the emulsion by a sudden drop in conductivity.

The effectiveness of the method is illustrated by seeking the optimum formulation for two crude oils in the presence of a mixture of an ionic EOR surfactant (sulfated propoxylated *n*-alcohol) and a nonionic

co-surfactant (ethoxylated *i*-alcohol), with or without alkali. Continuous salinity scan of the stirred SOW system maintained at constant temperature allows the identification of the optimal salinity within 30 minutes. This method therefore significantly accelerates the optimization of surfactant blends suitable for a given oil reservoir.

Keywords: Salinity Phase Inversion, Optimum formulation, EOR, Crude oil, Fast screening, Winsor III microemulsion

1. Introduction

Various scenarios try to shape the world energy demand in the next decades, taking into account the population growth, estimated at more than 9 billion people in 2040, and the climate change awareness. In particular, the evolution of the oil demand in the next decades is uncertain.

This global energy context along with crude oil prices volatility encourage oil producers to optimize the exploitation of their existing fields and to improve the efficiency of their extraction processes. In average, two-thirds of the oil remain trapped in a reservoir after primary and secondary (water flooding) recoveries. One technique to improve the recovery factor is the chemical Enhanced Oil Recovery (EOR) in which an aqueous solution of surfactants and polymers is injected inside the reservoir [1–3]. While polymers allow improving the mobility ratio, surfactants maximize oil mobilization and flow by reducing capillary forces [4]. To achieve an efficient desaturation, the interfacial tension between oil and water has to be reduced down to ultra-low values (~10^{-3} mN.m^{-1}), which can be achieved by finely tuning the surfactants blend. The conventional SP (Surfactant Polymer) and ASP (Alkali Surfactant Polymer) EOR processes aim at achieving very low residual oil saturations. Aside these processes that might be too demanding for full implementation on some fields, more easily deployable techniques using surfactants can be applied continuously or intermittently to improve oil production. For instance, well injectivity can be significantly improved by removing accumulated hydrocarbons near the wellbore [5]. This can be achieved by injecting low dosages – tens

of ppm of well-suited surfactants. Also, wellbore clean-up operations can be greatly improved by using well-designed mud cake remover formulations [6].

All these surfactant-based processes require to adjust the affinity of the surfactant blend to the oil to be extracted or to be removed. In all cases, the oil nature and the temperature of the process are fixed. One way to achieve the so-called “optimum formulation” is to change the salinity of the aqueous phase in order to modulate the relative affinity of the surfactant blend for water and for the targeted oil [7]. In some cases, because of the field constraints and of the water sources availability, the salinity is fixed also and the surfactants blend itself must then be adjusted to reach the optimum conditions.

In practice, the best surfactant system for a given reservoir is determined by salinity scans at the reservoir temperature and the optimum formulation is visually determined at the salinity for which a balanced Winsor III (noted WIII) microemulsion equilibrated system - containing equal volumes of oil and water - is obtained [8–10]. When the optimal salinity is out of the process-required range or if the Surfactant/Oil/Water (SOW) system does not form WIII systems, the surfactants blend is adjusted and new salinity scans are performed in order to check the phase behaviour over the salinity range. These scans require, in some cases, lengthy equilibrium times to unambiguously identify the phase behaviour with crude oil, which is a restricting factor to a fast determination of the appropriate surfactant system. Also, as mentioned, not all surfactant systems lead to three-phase microemulsion systems but rather form gels or viscous phases over the salinity gradient, which is highly undesirable [11,12].

The study presented in this paper shows that a fast determination of the optimum formulation in petroleum system can be achieved by dynamic Salinity-Phase-Inversion (SPI) of emulsions. By analysing the SPI curves obtained, it is possible to identify the optimum salinity and to anticipate the formation of WIII systems or not at equilibrium. This technique significantly speeds up the screening of surfactant systems for EOR and other surfactant-based improved oil recovery (IOR) processes.

2. Material and methods

2.1. Chemicals

The two crude oils studied - noted A and B - were supplied by TOTAL SA. Their main characteristics such as TAN, TBN, ASCI index, API degree, SARA fractions, viscosity and density at 25°C are listed in Table 1. TAN and TBN were measured according to the standard methods ASTM D664 [13] and ASTM D2896 [14] respectively. The ASCI index was determined with a specific method developed by TOTAL [15]. API degree was calculated from density extrapolated at 15°C and SARA fractions were determined by TLC-FID [16]. The EOR surfactants used in this study were developed and supplied by BASF. Two families of surfactants have been investigated: sulfated alkoxy *n*-alcohols (*n*-$C_{16\text{-}18}PO_kEO_jSO_4Na$) as main surfactants and ethoxylated *i*-alcohols (*i*-C_iEO_j) as co-surfactant. Their hydrophobic tails are either linear or branched and have between 10 and 18 carbons. The well-defined *n*-$C_{10}EO_4$ surfactant was synthesized in the lab and distilled to obtain an ultra-pure sample (> 99%) [17]. Bis(2-ethylhexyl) sulfosuccinate sodium salt, AOT (96%), *n*-Octane (≥ 99%), *n*-Decane (≥ 99%) and Toluene (≥ 99%) were purchased from Sigma Aldrich.

Table 1: *Characteristics of the crude oils studied*

Crude oil	**A**	**B**
TAN (mg KOH/g)[a]	0.5	2.0
TBN (mg eq KOH/g)[b]	1.7	2.5
ASCI index[c]	17	17
Viscosity at 25°C (mPa.s)	15.3	82.5
Density (25°C)	0.87	0.91
API degree[d]	31	23
Saturates (wt%)[e]	59.7	42.4
Aromatics (wt%)[e]	28.5	42.5
Resins (wt%)[e]	9.1	11.4
Asphaltenes(wt%)[e]	2.7	3.7

[a] *TAN = Total Acid Number*

[b] *TBN = Total Base Number*

[c] *ASCI =Asphaltene Solubility Class Index*

[d] *API = American Petroleum Institute*

[e] *SARA = Saturates, Aromatics, Resins, Asphaltenes*

2.2. Experimental procedure

2.2.1. SOW equilibrium behaviour

The phase behaviour of surfactants/oil/water systems was observed at WOR 1. Crude oils and model oils were used, and the water phase salinity was changed with NaCl with steps ranging from 1 g/L to 5 g/L depending on the systems. For crude oil-based systems, 1 mL of salted water containing the surfactant and the co-surfactant at the given concentration, with or without alkali (sodium carbonate or ammonia) was first poured in 5 mL-pipettes. Then, 1 mL of oil was added and the pipettes were sealed under a nitrogen flow and placed at the desired temperature for 10 minutes. They were then gently mixed and then mixed again after 1 hour, 2 hours and one night of equilibration. Observations of phase behaviour were made after complete stabilization (several days to several weeks). The optimal salinity was determined by plotting in the same graph the solubilisation of water in the microemulsion phase and the solubilisation of oil in the microemulsion phase, each divided by the total amount of surfactant and co-surfactant in the system, as a function of salinity [18,19]. The optimal salinity S* is the salinity at which the curves cross. The maximum uncertainty is estimated at ± 1 g/L. The solubilisation ratio at optimum σ^*, defined in Eq. 5, is also determined at this point.

2.2.2. Dynamic Salinity Phase Inversion (SPI)

Dynamic phase inversions were induced by increasing and decreasing continuously the aqueous phase salinity and were monitored by electrical conductivity measurement. Conductivity was recorded using a CDM210 conductivity meter from MeterLab® with a coupled conductivity-temperature electrode CDC641T from Radiometer Analytical®. Conductivity data were processed with the Labview software which records at the same time conductivity, temperature and the experimental time. The volume of the Surfactant/Oil/Water (SOW) mixtures varied during the experiment starting at 10 mL and finishing at 20 mL and the Water-to-Oil Ratio (WOR) was maintained equal to 1 (except for SPI experiments with $C_{10}EO_4$ and AOT in which the water mass fraction f_w is maintained to 0.5). The emulsification vessel was a 2.5 cm diameter * 20 cm height double-jacketed cylindrical tube. A 2 cm-

cross magnetic stirrer was used for agitation. The magnetic stirring rate was fixed at 900 rpm, which allowed obtaining reliable conductivity measurements in our systems, and the temperature was kept constant throughout the experiment by circulating water controlled by a HUBER 125 Ministat.

To continuously modify the salinity, an aqueous solution containing both the surfactant(s) and concentrated or diluted NaCl was added to the initial SOW mixture at a controlled flow rate Q_i of 0.05 mL/min thanks to a press-syringe engines model 78-8100INT from KdScientific® fitted with a 10-mL Terumo-syringe (reference SS+10ES1). Simultaneously, the crude oil was introduced in the same way at the same flow rate in order to maintain a constant WOR. Using a flow rate of 0.05 mL/min is a good compromise between the length of the experiment and a low impact of salinity variation kinetics on the determination of emulsion conductivity, as shown in Figure 1.

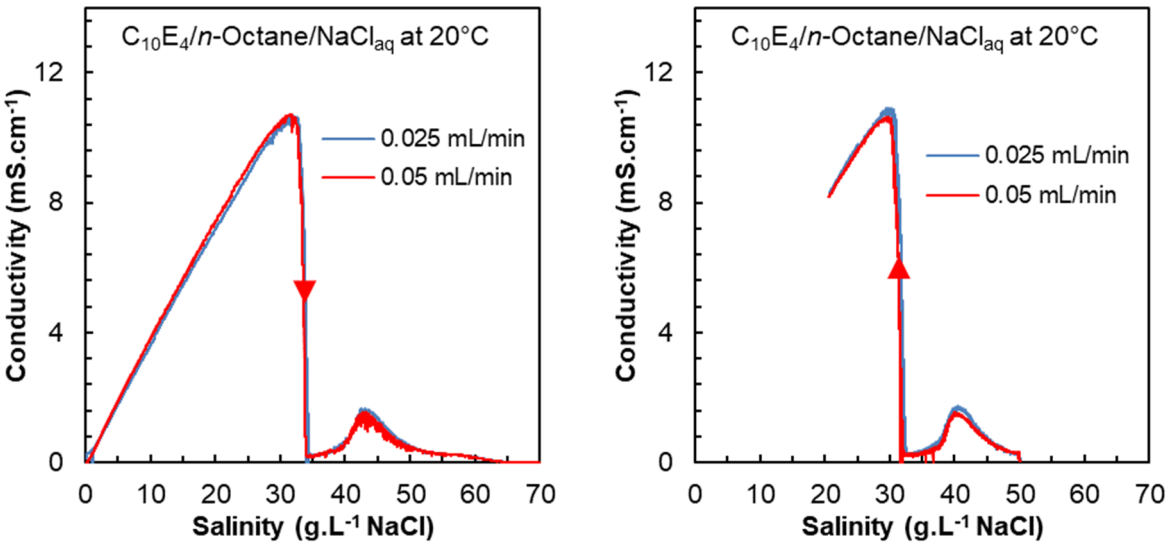

***Figure 1**: Impact of flow rate on the conductivity profile during a dynamic SPI experiment with an increase (left) and a decrease (right) of the aqueous phase salinity for the model system 3 wt.% $C_{10}EO_4$/n-Octane/$NaCl_{aq}$ system at 20°C at f_w = 0.5. The data have been recorded with a stirring rate of 900 rpm*

The procedure allows increasing or decreasing the aqueous phase salinity of the SOW sample under stirring without modifying the WOR nor the surfactant concentration, as illustrated in figure 2. Increasing the salinity of the aqueous phase requires dissolving large amounts of salt in an aqueous solution of surfactants, some of them being poorly salt-tolerant. Alternatively, two aqueous solutions

have to be injected, one containing the surfactant in low salinity brine, and the other one containing only a high concentration of salt. For simplification, the reverse procedure was implemented in this work, *i.e.* salinity was continuously decreased by adding a salt-free solution of surfactant to an initial SOW system with a high NaCl concentration. Such an experiment can be achieved within 30 minutes.

The aqueous phase salinity S(t), expressed in grams of NaCl per liter of aqueous phase, can be calculated at each time of the experiment by the following relation:

$$S(t) = \frac{S_0 V_0 + t.S_i Q_i}{V_0 + t.Q_i} \quad (1)$$

where S_0 and S_i are the initial and the added aqueous phase salinity respectively, t (in minutes) is the time, V_0 (in mL) the initial aqueous volume and Q_i (in $mL.min^{-1}$) the flow-rate of aqueous solution added to the SOW system. The SPI values are determined from the conductivity curves by using the parallel tangent methods and are given with a precision of ± 0.5 $g.L^{-1}$.

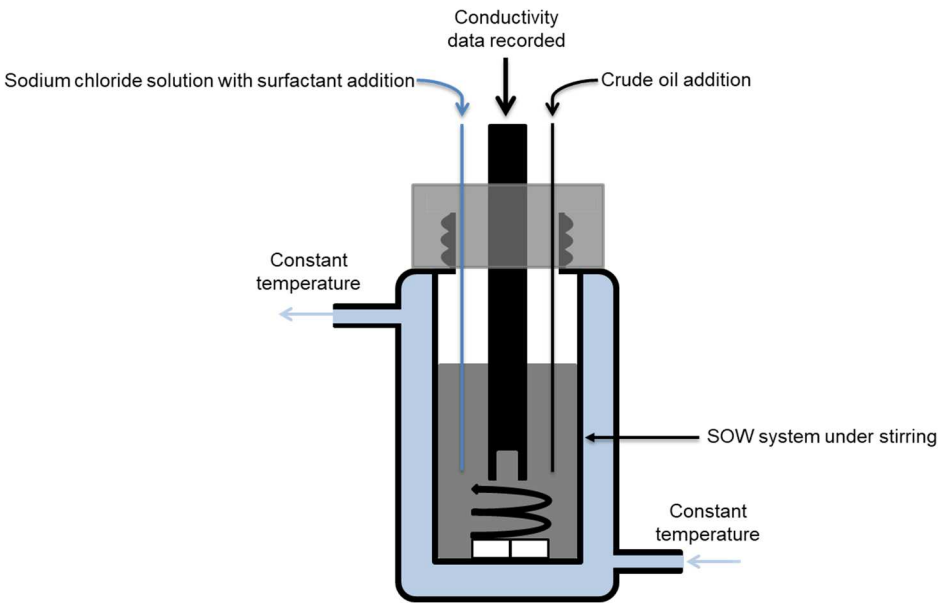

***Figure 2**: Experimental set up to achieve the dynamic SPI of Surfactant/Crude oil/Brine systems by increasing or decreasing the aqueous phase salinity*

169 ### 2.2.3. Interfacial tension

170 The interfacial tensions were measured with a spinning drop tensiometer SDT from KRÜSS GmbH®
171 allowing measurements down to 10^{-6} mN.m^{-1}. The measurements were carried out on equilibrated
172 SOW systems at 55 °C and at different fixed aqueous phase salinities. The various phases (aqueous,
173 oil and microemulsion phases) were first separated and were kept at 55°C during one hour before
174 interfacial tension measurements. For SOW systems exhibiting WI and WII microemulsion behaviours
175 at equilibrium, a droplet of the oil phase (between 2 and 10 µL) was inserted in the capillary filled
176 with 1 mL of the aqueous phase. For WIII microemulsion systems, a 2 µL droplet of the oil phase in
177 excess was inserted with a small amount of the middle-phase microemulsion (less than 1 µL in
178 average) within the capillary filled with 1 mL of the aqueous phase in excess in order to get stable and
179 accurate interfacial tension values as recommended in the literature [20]. All interfacial tension
180 measurements were made after complete stabilisation of the SOW system inside the capillary and
181 repeated on more than 5 droplets by using the Young-Laplace equation (Eq. 2).

182 $$\Delta P = 2\gamma H = \gamma\left(\frac{1}{R_1} + \frac{1}{R_2}\right) \quad (2)$$

183 where ΔP is the Laplace pressure difference across the interface, γ the interfacial tension, H the mean
184 curvature, and R_1 and R_2 are the principal radii of curvature [21]. For each individual droplet, the
185 interfacial tension values are measured with a precision of ± 1.10^{-6} mN.m^{-1} according to the supplier.
186 The values given are means values on 5 droplets and the mean deviation is 30% for WIII systems and
187 20% for WI and WII systems in average.

188

189 ## 3. Results and discussion

190 In this section, after a description of the different detection methods, we show how the SPI method
191 allows characterizing model SOW systems. Then, it is applied to petroleum SOW systems and we
192 show the close correspondence between the SPI and the optimal salinity determined at equilibrium.
193 We also demonstrate that the SPI method allows anticipating the formation of viscous phases.

3.1. Detection methods of the phase inversion

The so-called "standard" phase inversion is traditionally detected by emulsifying a series of tubes containing a SOW system pre-equilibrated at various temperatures or salinities [22]. The type of emulsion is then determined by conductimetry to identify the inversion border. It can also be determined in a dynamic way by applying a continuous variation of one of the formulation parameters to a stirred system. Dynamic experiments are usually performed using temperature as the formulation variable because it can easily and reversibly be changed in a controlled manner. The easiest way to determine the dynamic phase inversion transition of emulsions is to record the conductivity signals [23–33]. At the phase inversion, the SOW system reverses itself by giving a complex mixture of microemulsion, oil and water, which is less conductive than the previous O/W emulsion. It induces a fall in conductivity. After the phase inversion, the SOW system shows a conductivity close to zero because a W/O emulsion is obtained. The phase inversion is then defined as the temperature at which the fall in conductivity occurs. The dynamic method provides significant time savings compared to the equilibrium scan, a dramatic signal visualization of the phase inversion and a margin of error close to zero compared to the discontinuous equilibrium procedure with a series of pipettes [27]. The phase inversion can also be detected by viscosity measurements [34–38] or by light backscattering and near-infrared spectroscopy [39,40], as the light backscattering intensity strongly depends on the droplet size of the stirred emulsion [41,42].

3.2. The Dynamic Salinity Phase Inversion (SPI) with model oils and surfactants

The transitional phase inversion is defined as the change in the emulsion morphology from an oil-in-water (O/W) to a water-in-oil (W/O) emulsion, and vice versa, resulting from the change of the surfactant affinity from water to oil. This affinity change can be induced by modifying any formulation variable. Historically, temperature was used for polyethoxylated surfactant-based systems [23,24,43] but other variables like the number or ethoxy groups or the length of the hydrophobic tail of the surfactant, the nature and the concentration of alcohol in the blend, as well as the salinity of the

aqueous phase can also be used as variable parameters [25,26,44]. In the same way, numerous studies have evidenced that the phase inversion, induced by temperature or salinity, occurs within the WIII zone at equilibrium for model oils [25,26,45–49] and also for crude oils by taking temperature as formulation variable [34,50]. This result is valid whatever the type of surfactant if the volume Water-to-Oil Ratio (WOR) of the SOW system is close to 1 as shown in the literature for ionic [26] and nonionic [27,51,52] surfactants. This result is also valid even for mixtures of technical grade ionic and nonionic surfactants with variations of the proportion of surfactants in the mixture, as demonstrated by Antón *et al.* [53]. In addition to the WOR, other parameters can impact the identification of the optimum formulation by dynamic phase inversion. In particular, a too-low surfactant concentration, an inefficient stirring as well as a very high viscosity of the oil can impact the phase inversion conductivity signal and induce hysteresis (different inversion location depending on the way the formulation variable is changed), as highlighted by Márquez *et al.* in Temperature-induced phase inversion of non-ionic surfactants-based systems [54]. It means that, for suitable WOR, surfactant concentration, stirring and oil viscosity ranges, the phase inversion can be used to identify rapidly the optimum formulation for model oils (figure 3) [55] and also for crude oils when temperature is changed in a dynamic way [34,50].

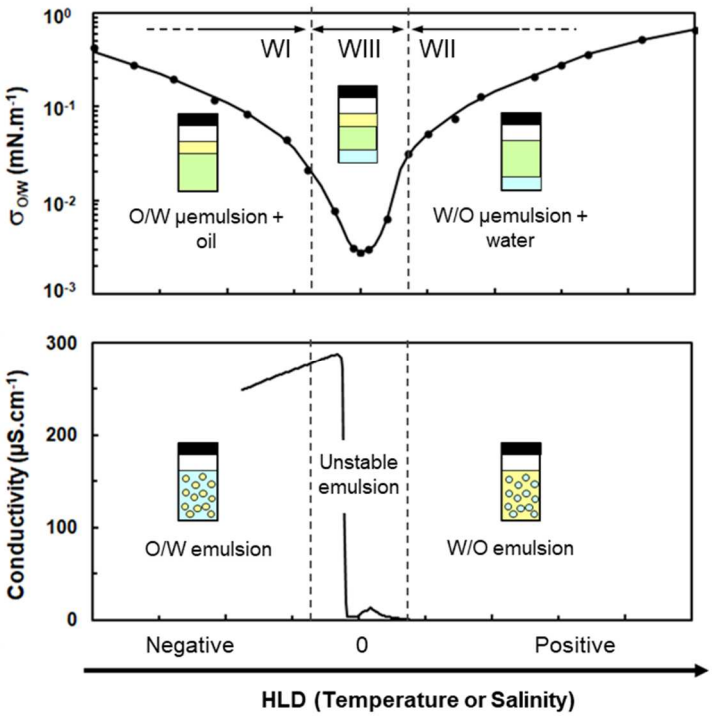

***Figure 3**: Characteristic phenomena occurring close to the "optimum formulation" for (top) Equilibrated system: deep minimum of W/O interfacial tension and three-phase system with a middle microemulsion phase containing the same amount of oil and water and (down) Emulsified system: O/W, unstable, or W/O emulsion depending on whether the system is emulsified before, at, or after the optimum formulation and phase inversion of the same stirred system detected by a sudden drop of conductivity. Reproduced with authorization from Ref [55]*

In a first step, the phase inversion induced by continuous salinity change was studied for two SOW model systems: the nonionic $C_{10}EO_4$/*n*-Octane/$NaCl_{(aq)}$ and the ionic AOT/*n*-Decane/$NaCl_{(aq)}$.

For these simple SOW systems, the optimum salinities S* can be approximately estimated with the Hydrophilic Lipophilic Deviation (HLD) equations from *Salager et al* (Eq. 3 for nonionics and 4 for ionics) [22].

$$HLD = (\alpha - EON) - k.EACN + t.\Delta T + b.S^* + f(A) = 0 \; at \; optimum \; formulation \quad (3)$$

$$HLD = \sigma - k.EACN + t.\Delta T + \ln(S^*) + f(A) = 0 \; at \; optimum \; formulation \quad (4)$$

Where:

- α, σ, EON, k, and t are parameters depending on the surfactant,
- S (wt%) is the salinity of the aqueous phase,
- EACN is the equivalent alkane carbon number of the oil,
- ΔT (°C) is the temperature deviation from 25 °C,
- A (wt%) is the alcohol concentration and f(A) a function depending on the alcohol type.

The HLD relation establishes that the optimal salinity S* and the optimal temperature are correlated in a logarithmic scale for ionic surfactants and in a linear way for nonionics. These equations predict that an optimal salinity of ≈ 22 $g.L^{-1}$ at 20°C for the nonionic system and ≈ 6 $g.L^{-1}$ at 40°C for the ionic system are required to reach the optimum formulation (calculations are detailed in the supplementary information) [22,33,56]. These systems were studied by continuously modifying the salinity to trigger the phase inversion. Figure 4 shows the conductivity vs salinity profiles for the nonionic (left) and ionic (right) systems. The vertical dotted lines in the figure indicate the frontiers of the different phase behaviors at equilibrium (WI, WIII and WII). For the 3 wt. % $C_{10}EO_4$/*n*-Octane/$NaCl_{(aq)}$ system, the inversion was studied both in dynamic (solid curves) and standard (dotted curve) mode. For the dynamic inversion, conductivity was monitored either by continuously increasing or decreasing the aqueous salinity (blue and red curves respectively in figure 4 left). For the standard inversion mode, the conductivity was measured after emulsification of pre-equilibrated samples at different salinities (black points in figure 4 left).

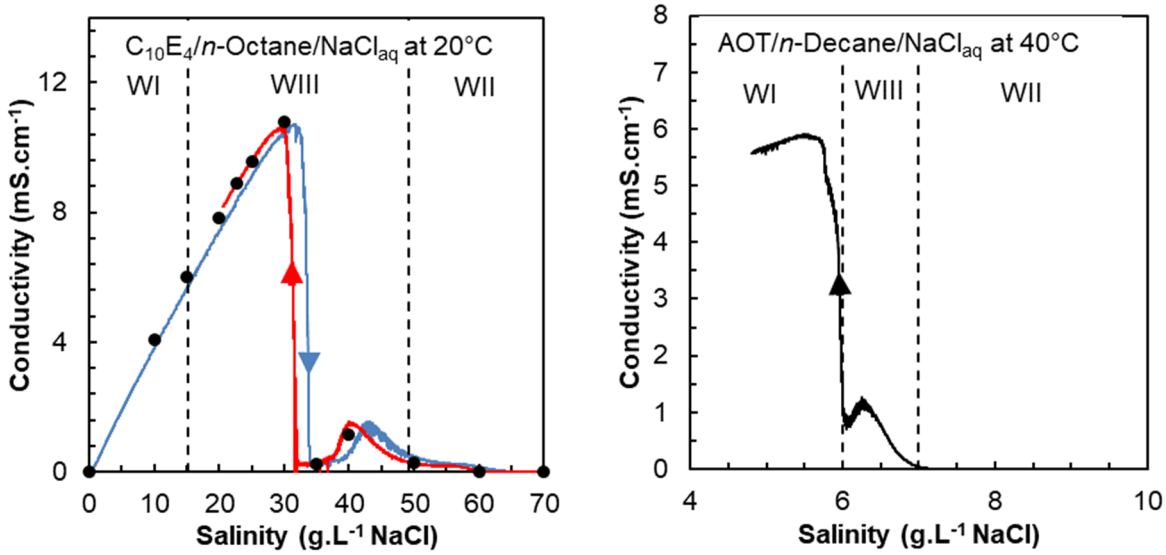

***Figure 4**: (Left) SPI of the 3 wt.% $C_{10}EO_4$/*n*-Octane/$NaCl_{aq}$ system at 20°C with f_w = 0.5 monitored by conductivity by continuously increasing (blue curve) or decreasing (red curve) the salinity, and after mixing samples initially at equilibrium (black dots) (Right) SPI of the 5 wt.% AOT/*n*-Decane/$NaCl_{aq}$ system at 40°C with f_w = 0.5 monitored in conductivity by decreasing the aqueous salinity. The equilibrium phase behavior (WI, WII or WIII) zones at different salinities are indicated in both figures (black dotted vertical lines).*

As displayed in figure 4 (left), the SPI occurs in the salinity range 31-34 $g.L^{-1}$ NaCl depending on the protocol used. This range value is somewhat higher than the value anticipated by the HLD equation. However, the dynamic SPI occurs within the WIII region, showing the effectiveness of this technique which can be used to identify rapidly the optimum formulation conditions of SOW systems based on nonionic surfactants. The profile of the blue curve follows the expected tendency, *i.e.* an increase of conductivity almost proportional to the NaCl concentration until a sharp drop when the morphology of the emulsion changes from O/W to W/O. The conductivity signal shows non-zero values between 35 and 60 $g.L^{-1}$ NaCl with a slight maximum centered at 43 $g.L^{-1}$ NaCl. This bump appears regardless the protocol used (continuous or discontinuous scan), indicating that it is not due to artefacts but results from the complex morphology of the three-phase emulsion Water/Microemulsion/Oil formed by agitation of the WIII system.

The S* values determined by increasing or decreasing the salinity differ from 3 $g.L^{-1}$ NaCl. This small hysteresis could be due to the deviation from WOR = 1 when brine or pure water is added to the emulsion since the WOR is known to slightly influence the transitional phase inversion of emulsions [27]. For the same reason, the optimal salinity found by the discontinuous scan (black dots) differs slightly from that obtained under dynamic conditions. The dynamic SPI can be also used to identify the optimum salinity for ionic surfactants as demonstrated by figure 4 (right) for the 5 wt.% AOT/*n*-Decane/$NaCl_{(aq)}$ system at 40°C. For this system, the conductivity drop and the residual conductivity detected after the inversion coincides exactly with the WIII region observed at equilibrium, which confirms the close correspondence between the optimum formulation at equilibrium and the continuous SPI. The experimental SPI value of 6 $g.L^{-1}$ NaCl matches very well with the value predicted from the HLD equation but it slightly differs from the optimal salinity (7 to 9 $g.L^{-1}$) reported by Kahlweit *et al.* for the same system [57]. Indeed, several artefacts can modify the experimental value of S* especially when the WIII domain is narrow as for the AOT/*n*-Decane/$NaCl_{(aq)}$ system. Firstly, the gradual addition of pure water (decreasing salinity) to the initial SOW system changes a little bit the surfactant concentration (see figure 1 in supplementary information). Secondly, AOT (purity 96%) is a diester which may contain small amounts of the starting material (ethylhexyl alcohol) and can undergo some hydrolysis during storage. It is well known that even a small amount of this branched alcohol can play the role of co-surfactant and significantly shift the value of S* [22,58,59].

3.3. The dynamic SPI for EOR applications

3.3.1. Correspondence between phase behavior, emulsion inversion and interfacial tension minimum

The addition of well-chosen surfactants modifies the phase behavior of crude oil/water system and may eventually lead to the formation of three-phase microemulsion systems (WIII) in which the oil/water interfacial tension reaches an ultra-low value [60,20,22]. Such systems can be obtained by

balancing the surfactant affinity for the aqueous and oil phases to suit the crude oil under study. As already mentioned, the modification of the surfactant affinity can be made by adding a suitable co-surfactant or by tuning the temperature and/or the salinity [61].

In the EOR field, temperature is fixed by the reservoir temperature, and so salinity remains the preferred variable parameter to adjust the surfactant affinity. In that way, the optimum formulation is determined by discontinuous salinity scans carried out at equilibrium and at the reservoir temperature. From this salinity scan at equilibrium, it is possible to determine the optimum salinity S* but also the efficiency of the surfactant system, which is evidenced by the microemulsion volume related to the volume of surfactant used. To express this efficiency, the solubilization ratio σ*, expressed in cm^3/cm^3 or cc/cc, is often used (Eq. 5) [4,62]. F

$$\sigma^* = \frac{V_{O\ or\ W/\mu}}{V_S} = \frac{Volume\ of\ water\ or\ oil\ in\ the\ microemulsion\ at\ optimum}{Volume\ of\ surfactant + co{-}surfactant\ \ in\ the\ system} \quad (5)$$

From the solubilization ratio, it is also possible to infer the minimum interfacial tension at the optimum formulation by considering the model proposed by Huh displayed in Eq. 6 [18]:

$$\frac{\sigma^{*2}.\gamma^*}{\cos(\frac{\pi}{4})} = a_H \quad (6)$$

where σ* (cc/cc) is the solubilization ratio, γ* ($mN.m^{-1}$) is the minimum of interfacial tension, and a_H ($mN.m^{-1}$) is a parameter that depends on the surfactant type.

a_H has already been calculated for series of surfactants [63–65] and can be approximated to 0.42 $mN.m^{-1}$ in most cases. Therefore, the Huh's equation is often used in its simplified form (Eq. 7) [66]:

$$\gamma^* = \frac{0.3}{\sigma^{*2}} \quad (7)$$

Solubilization ratios higher than 10 cc/cc are usually desired for EOR applications, to ensure that sufficiently low interfacial tension values are attained.

As the dynamic SPI method allows finding the "optimal conditions" for model systems, this technique deserves to be tested on systems relevant to EOR applications, for which the optimum salinity is a key parameter. In order to evaluate the feasibility of the SPI with petroleum-based systems, a mixture of a sulfated alkoxylated alcohol surfactant, a nonionic co-surfactant, a typical crude oil and brine was studied. Figure 5 shows the conductivity vs. salinity profile for the [*n*-$C_{16\text{-}18}PO_4SO_4Na$ + *i*-$C_{13}EO_{13}$]/Crude oil A/Brine at WOR=1. Additionally, the O/W interfacial tensions measured on equilibrated systems with a spinning-drop tensiometer at different salinities are also shown.

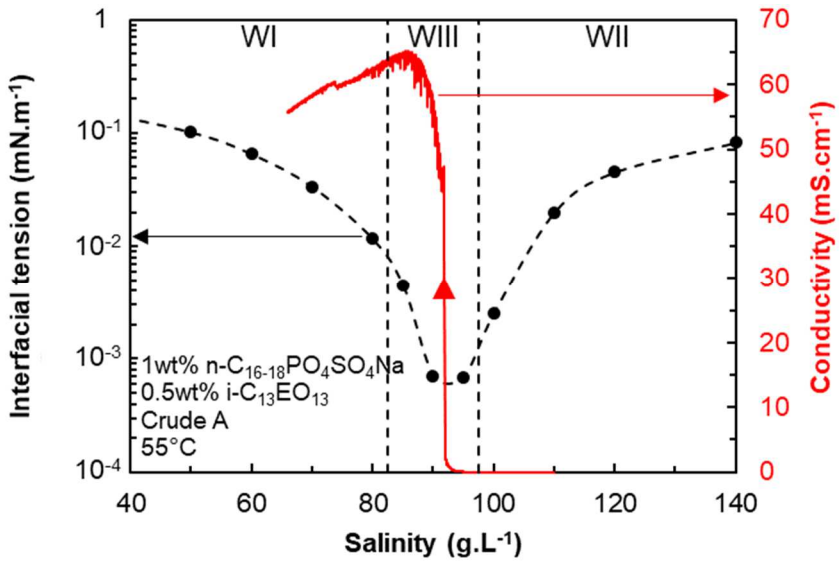

***Figure 5**: Identification of the "optimum salinity" S* of a crude oil based SOW system by dynamic SPI monitored by conductimetry while decreasing the aqueous salinity (red curve). Evolution of the W/O interfacial tension (black dots and dashed curve) and limits of the WIII region (black dotted vertical lines)*

As can be seen in figure 5, the dynamic SPI coincides exactly with the minimum interfacial tension. As for model SOW system, the sharp drop in conductivity occurs within the salinity range where the WIII microemulsion system at equilibrium is obtained with ultra-low interfacial tension values close to 5.10^{-4} mN.m^{-1}. By comparison, the Huh equation gives a value of $2.5.10^{-3}$ mN.m^{-1} for this system according to the solubilization ratio at equilibrium (11 cc/cc). This predicted value is significantly higher than the measured IFT value, which indicates that the a_H parameter commonly taken in the Huh's model overestimates the interfacial tension value at optimum for this surfactant system. Anyway, this experiment highlights that the SPI actually occurs at the optimum formulation, even for SOW systems composed of crude oils and mixtures of ionic/nonionic technical grade surfactants.

The evolution of the interfacial tension appears to be similar to the one reported in literature using salinity as formulation variable for ionic surfactants [67,68] and temperature [20] or the number of ethylene oxide groups for nonionic surfactants [69].

3.3.2. Effect of formulation on the formation of viscous phases for equilibrated SOW systems

One difficulty often encountered when formulating surfactant blends for EOR is that some crude oils form undesirable viscous phases instead of the fluid WIII systems. To overcome this problem, the formulation must be modified. In practice, an alkali is often used to reveal the endogenous surfactants and/or significant amounts of a co-solvent are added to the formulation in order to make the interfacial film more fluid [70–72]. Barnes *et al.* have shown that a given surfactant formulation matches well, moderately or badly the oil (*i.e.* it forms WIII systems, loose or viscous gel phases respectively) depending on the crude chemical nature and they have tried to relate these behaviours with some bulk analytical descriptors of the oil [12]. Crude oils also contain naphthenic acids and asphaltenes [11] acting as endogenous surfactants that play a role in the SOW phase behaviour in the presence of

synthetic surfactants [73]. This effect is particularly sensitive for high TAN crude oils in the presence of alkali because naphthenic acids are converted into highly surface active naphthenates.

Table 2 shows some surfactant formulations studied at equilibrium with crude A (entries a-j) and crude B (entries k-r). They are all based on a mixture of an ionic surfactant *n*-$C_{16-18}PO_kEO_jSO_4Na$ and a nonionic co-surfactant (i-C_iEO_j) or 2-Butanol, with or without alkali (sodium carbonate or ammonia). This set of experiments has been built starting from the conditions described in figure 5 with crude A (entry a). The initial formulation has been changed to study the influence of the formulation variables on the optimal salinities S* and on the efficiencies of the surfactant systems (solubilisation ratio values σ^* or formation of viscous phases). These effects are summarized in Table 3.

Table 2*: Experimental values obtained for optimum salinity at equilibrium S* and solubilization ratio at optimum σ* for the different petroleum SOW systems tested*

Entry	Crude	Ionic surfactant		Co-surfactant		Alkali		T	S*	σ*
		Formula	wt.%	Formula	wt.%	Type	wt.%	°C	g.L^{-1}	cc/cc
a	A	*n*-$C_{16-18}PO_4SO_4Na$	1	*i*-$C_{13}EO_{13}$	0.5	-	-	55	89	11
b	A	*n*-$C_{16-18}PO_4SO_4Na$	1	*i*-$C_{10}EO_{10}$	0.33	-	-	55	60-70[§]	N/A
c	A	*n*-$C_{16-18}PO_4SO_4Na$	1	*i*-$C_{10}EO_{10}$	0.5	-	-	55	85	10
d	A	*n*-$C_{16-18}PO_4SO_4Na$	1	*i*-$C_{10}EO_{10}$	1	-	-	55	110	5
e	A	*n*-$C_{16-18}PO_4SO_4Na$	1	*i*-$C_{13}EO_{10}$	0.5	-	-	55	55-70[§]	N/A
f	A	*n*-$C_{16-18}PO_4SO_4Na$	1	*i*-$C_{17}EO_{12}$	0.5	-	-	55	50-70[§]	N/A
g	A	*n*-$C_{16-18}PO_4SO_4Na$	1	2-BuOH	1.5	-	-	55	40-45[§]	N/A
h	A	*n*-$C_{16-18}PO_2SO_4Na$ / *n*-$C_{16-18}PO_4SO_4Na$ (50/50)	1	*i*-$C_{13}EO_{13}$	0.5	-	-	65.5	81	9
i	A	n-$C_{16-18}PO_2SO_4Na$ / *n*-$C_{16-18}PO_4SO_4Na$ (50/50)	1	*i*-$C_{13}EO_{13}$	0.5	Na_2CO_3	0.5	65.5	70	10
j	A	*n*-$C_{16-18}PO_2SO_4Na$ / *n*-$C_{16-18}PO_4SO_4Na$ (50/50)	1	*i*-$C_{13}EO_{13}$	0.5	$NH_{3,aq}$	0.5	65.5	70	13
k	B	*n*-$C_{16-18}PO_4SO_4Na$	1	*i*-$C_{13}EO_{13}$	0.5	Na_2CO_3	0.5	40	150	8
l	B	*n*-$C_{16-18}PO_4SO_4Na$	1	*i*-$C_{13}EO_{13}$	0.5	Na_2CO_3	0.5	55	134	8

m	B	*n*-$C_{16\text{-}18}PO_4SO_4Na$	1	*i*-$C_{13}EO_{13}$	0.5	Na_2CO_3	0.5	65	120	7
n	B	*n*-$C_{16\text{-}18}PO_7EO_{0.1}SO_4Na$	1	*i*-$C_{13}EO_{13}$	0.25	Na_2CO_3	0.5	55	68	22
o	B	*n*-$C_{16\text{-}18}PO_7EO_{0.1}SO_4Na$	0.5	*i*-$C_{13}EO_{13}$	0.125	Na_2CO_3	0.5	55	79	20
p	B	*n*-$C_{16\text{-}18}PO_7EO_{0.1}SO_4Na$	0.25	*i*-$C_{13}EO_{13}$	0.0625	Na_2CO_3	0.5	55	81	24
q	B	*n*-$C_{16\text{-}18}PO_7EO_{0.1}SO_4Na$	0.25	*i*-$C_{13}EO_{13}$	0.0625	$NH_{3,aq}$	0.5	55	55	40
r	B +14% Toluene	*n*-$C_{16\text{-}18}PO_7EO_{0.1}SO_4Na$	0.25	*i*-$C_{13}EO_{13}$	0.0625	Na_2CO_3	0.5	55	55	30

§No WIII, gels formed instead in the salinity range indicated in the S* column.

Table 3*: Effect of the main formulation variable changes on the phase behavior of the SOW systems described in Table 2*

Parameters	Entries	Formulation change	S*	σ*
Amount of co-surfactant	b → c → d	% *i*-$C_{10}EO_{10}$ ↗	↗↗	↘↘
Type of co-surfactant	a → c	*i*-$C_{13}EO_{13}$ → *i*-$C_{10}EO_{10}$	≈	≈
	c → e	*i*-$C_{10}EO_{10}$ → *i*-$C_{13}EO_{10}$	⇨ gel phase	NA
	c → f	*i*-$C_{10}EO_{10}$ → *i*-$C_{17}EO_{12}$	⇨ gel phase	NA
	c → g	*i*-$C_{10}EO_{10}$ → 2-BuOH	⇨ gel phase	NA
Base to reveal endogenous surfactants	h → i	+ Na_2CO_3 (crude A)	↘	≈
	h → j	+ $NH_{3,aq}$ (crude A)	↘	↗
	p → q	Na_2CO_3 → $NH_{3,aq}$ (crude B)	↘↘	↗↗
Temperature	k → l → m	Temperature ↗	↘	≈
Amount of {surfactant + co-surfactant}	n → o → p	%{surfactant + co-surfactant}↘	↗	≈
Type of oil	p → r	% Toluene ↗	↘↘	↗↗

Amount and type of co-surfactant:

For crude A, poor in naphthenic acids and asphaltenes, the addition of alkali is not essential to obtain a WIII system but the nature and the amount of nonionic co-surfactant has to be adapted to avoid the formation of gel phases. A ratio surfactant/co-surfactant of 2 is convenient when the co-surfactant is *i*-$C_{13}EO_{13}$ (entry a) or *i*-$C_{10}EO_{10}$ (entry c). In contrast, the less hydrophilic co-surfactants *i*-$C_{13}EO_{10}$ (entry e) or *i*-$C_{17}EO_{12}$ (entry f) [34] lead to the formation of gel phases. Increasing the amount of

nonionic co-surfactant *i*-$C_{10}EO_{10}$ is a lever to overcome the formation of gel phases (see entries b-d) but it has a negative impact on the solubilisation ratio. Using a simple alcohol (2-butanol), even in large amounts, is not sufficient to avoid the formation of gel phases without alkali (entry g).

Revelation of endogenous surfactants with alkali:

Crude B contains a significant amount of naphthenic acids according to its TAN value (see Table 1). It is a more "difficult" oil than crude A because it is significantly more viscous and because it is particularly prone to the formation of gel phases. For crude oil B, the addition of an alkali is necessary to obtain WIII systems with these surfactants blends. The naphthenates formed at high pH probably act as anionic co-surfactants and promote the formation of fluid interfaces. On the contrary, crude A that has a relatively low TAN (see Table 1) does not require the systematic use on alkali to obtain WIII systems. The addition of either sodium carbonate or ammonia induces a slight decrease of the optimal salinity (entries h-j). For crude B, the impact of alkali is much more pronounced. First, a decrease of the total concentration of exogenous surfactant and cosurfactant at a constant Na_2CO_3 concentration (entries n-p) induces a significant increase of the optimal salinity.

The increase in hydrophilic character of the surfactant blend could have several origins. Exogenous surfactants are not pure but technical grade compounds, and a change in concentration can lead to a change in the nature of the surfactants present at the interface (more hydrophilic in this case) due to different partition coefficients. Another hypothesis is the contribution of hydrophilic naphthenates because their relative amount (compared to exogenous surfactants) increases. It can also result from a combination of both effects. The second noticeable impact is the nature of the alkali. The addition of $NH_{3,aq}$ make the surfactant blend much more hydrophobic (compare S* for entries p and q), which can be due to different natures and/or amounts of the endogenous surfactants revealed. The values of solubilisation ratios obtained for crude B in the presence of alkali are only apparent and are overestimated since the naphthenates formed are not taken into account in the calculation.

Extrapolation to Reservoir conditions:

441 The SOW phase behaviour needs to be extrapolated to reservoir conditions. Temperature has an
442 important effect on the optimal salinity (entries k-m) for these systems. An increase in temperature
443 leads to a decrease of the optimum salinity because surfactants loose hydrophilicity, in agreement with
444 previous studies with crude oils [34]. It does not impact the efficiency of the surfactant system,
445 because of this negative salinity shift, as evidenced by the constant solubilisation ratios. To take into
446 account the modification of the oil physical chemistry induced by the dissolution of gases in the (P,T)
447 reservoir conditions, surrogate oils are usually prepared by blending the dead crude oil with a defined
448 amount of solvent. Toluene is usually chosen because its EACN equals 1 and it is therefore a good
449 substitute of methane at ambient pressure [74]. As expected, adding a significant amount of toluene to
450 crude B in order to mimic the properties of the live oil induces a decrease of the optimal salinity and
451 an increase of the solubilisation ratio (see entries p and r).
452
453 **3.3.3. Identification of the formation of viscous phases by continuous SPI experiments**
454 To evidence that the dynamic SPI can be an effective tool for optimizing surfactant blends for EOR,
455 the SPI has been determined for a selection of the SOW systems described in Table 2 (entries a-g, k-
456 m, o-p and r). Experimental results are gathered in Table 4.
457
458 ***Table 4**: Petroleum-based SOW systems investigated by dynamic SPI. The SPI column shows the*
459 *salinity values at which the phase inversion is observed. Columns S* and σ* correspond to the value*
460 *determined for the same system at equilibrium*

Entry	Crude	Ionic surfactant		Co-surfactant		Alkali		T	S*	σ*	SPI
		Formula	wt.%	Formula	wt.%	Type	wt.%	°C	g.L^{-1}	cc/cc	g.L^{-1}
a	A	*n*-$C_{16\text{-}18}PO_4SO_4Na$	1	*i*-$C_{13}EO_{13}$	0.5	-	-	55	89	11	91
b	A	*n*-$C_{16\text{-}18}PO_4SO_4Na$	1	*i*-$C_{10}EO_{10}$	0.33	-	-	55	60-70§	N/A	77
c	A	*n*-$C_{16\text{-}18}PO_4SO_4Na$	1	*i*-$C_{10}EO_{10}$	0.5	-	-	55	85	10	91
d	A	*n*-$C_{16\text{-}18}PO_4SO_4Na$	1	*i*-$C_{10}EO_{10}$	1	-	-	55	110	5	114
e	A	*n*-$C_{16\text{-}18}PO_4SO_4Na$	1	*i*-$C_{13}EO_{10}$	0.5	-	-	55	55-70§	N/A	73§
f	A	*n*-$C_{16\text{-}18}PO_4SO_4Na$	1	*i*-$C_{17}EO_{12}$	0.5	-	-	55	50-70§	N/A	64§
g	A	*n*-$C_{16\text{-}18}PO_4SO_4Na$	1	2-BuOH	1.5	-	-	55	40-45§	N/A	49§

k	B	*n*-$C_{16\text{-}18}PO_4SO_4Na$	1	*i*-$C_{13}EO_{13}$	0.5	Na_2CO_3	0.5	40	150	8	150
l	B	*n*-$C_{16\text{-}18}PO_4SO_4Na$	1	*i*-$C_{13}EO_{13}$	0.5	Na_2CO_3	0.5	55	134	8	127
m	B	*n*-$C_{16\text{-}18}PO_4SO_4Na$	1	*i*-$C_{13}EO_{13}$	0.5	Na_2CO_3	0.5	65	120	7	110
o	B	*n*-$C_{16\text{-}18}PO_7EO_{0.1}SO_4Na$	0.5	*i*-$C_{13}EO_{13}$	0.125	Na_2CO_3	0.5	55	79	20	80
p	B	*n*-$C_{16\text{-}18}PO_7EO_{0.1}SO_4Na$	0.25	*i*-$C_{13}EO_{13}$	0.0625	Na_2CO_3	0.5	55	81	24	85
r	B +14% Toluene	*n*-$C_{16\text{-}18}PO_7EO_{0.1}SO_4Na$	0.25	*i*-$C_{13}EO_{13}$	0.0625	Na_2CO_3	0.5	55	55	30	53

[§]No WIII, gels formed instead in the salinity range indicated in the S* column. The SPI values are determined at the negative spike (see figure 6)

In a previous work, we have shown that there is a correspondence between the conductivity profile obtained during the dynamic PIT of petroleum systems and their ability to form WIII systems at equilibrium [34]. Figure 5 and Figure 6 show that it holds true when the inversion is induced by a continuous variation of salinity. The system based on *n*-$C_{16\text{-}18}PO_4SO_4Na$ 1 % / *i*-$C_{13}EO_{13}$ 0.5 % (Table 4 entry a, figure 5) forms WIII systems at equilibrium and shows a complete inversion on the dynamic SPI conductivity profile. On the contrary, the system based on *n*-$C_{16\text{-}18}PO_4SO_4Na$ 1 % / *i*-$C_{17}EO_{12}$ 0.5 % (Table 4 entry f, figure 6) does not form WIII systems at equilibrium but rather gel phases on a certain range of salinities. During the dynamic SPI, no clean inversion is observed, however an accident on the conductivity curve is clearly visible. The same behavior occurs for all systems that do not form WIII systems at equilibrium (entries e-g of table 4) except for the system of entry b, which will be discussed in the following section.

The salinity at which the conductivity shows a negative spike is related to the zone of gel phase formation at equilibrium. For these systems, the oil/water interfacial tension is reduced when approaching the optimal salinity range ($3.6.10^{-2}$ $mN.m^{-1}$ measured for the system described in Table 4, entry f at 65 g/L), however, it does not reach ultra-low values. We can suppose that the co-surfactant chosen in this case is not suitable to promote a fluid interface allowing the inversion of the emulsion during the dynamic salinity scan and the formation of a WIII system at equilibrium.

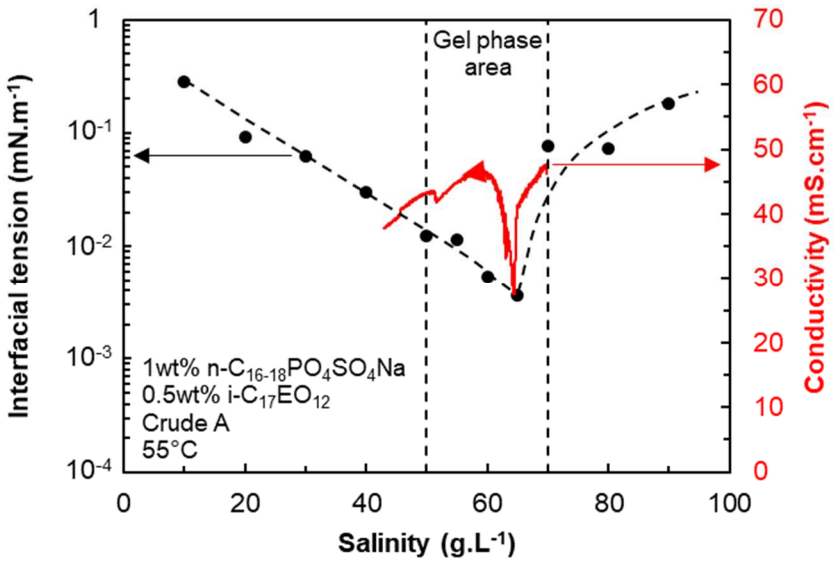

***Figure 6**: Identification of the optimum salinity range of a SOW system exhibiting viscous phases at equilibrium (entry f of Table 4) by dynamic SPI monitored by conductimetry while decreasing the aqueous salinity (red curve). Evolution of the W/O interfacial tension (black dots and dashed curve) and gel phase area borders (back dotted vertical lines)*

From a practical point of view, the shape of the conductivity profile during a dynamic SPI can be used as a descriptor of the phase behaviour of petroleum SOW systems regarding their ability to form a WIII microemulsion system or not.

3.3.4. Use of the dynamic SPI to quantify the influence of formulation variables on the position of the optimum

Also, the dynamic SPI reveals to be a valuable tool to quantify the influence of cross-parameters on the optimum formulation. Figures 7 and 8 illustrate the impact of temperature and co-surfactant concentration respectively.

Figure 7 shows the conductivity profiles during the dynamic SPI of the *n*-$C_{16\text{-}18}PO_4SO_4Na$ 1 % / *i*-$C_{13}EO_{13}$ 0.5 % with crude B in the presence of Na_2CO_3 (Table 3, entries k-m). A temperature increase leads to a decrease of S* at equilibrium and of the SPI under dynamic conditions. Increasing

502 temperature decreases the hydrophilicity of the polyethoxylated nonionic co-surfactant due to the
503 progressive dehydration of the polyethoxylated polar head. The same effect occurs for the
504 propoxylated groups of the hybrid anionic propoxylated sulfate, whereas the ionic head itself becomes
505 more hydrophilic with increasing temperature.

506 The fact that the addition of propoxylated groups within a homogeneous series of ionic surfactants
507 decrease the global hydrophilicity towards temperature means that propoxylated groups are more
508 impacted by temperature changes than the ionic head [34,50]. As a consequence, the salinity needed to
509 attain the optimum conditions is lower because the temperature increase has made the surfactant
510 system more hydrophobic, as already mentioned by Hammond *et al*. with the same class of surfactants
511 and model oils [75]. The linear evolution of the SPI value with temperature (insert in figure 7)
512 indicates that the surfactant blend as a whole shows a nonionic-type dependence towards temperature
513 (HLD Eq. 3).

514 It is important to stress that these dynamic SPI experiments have been performed by continuously
515 decreasing the salinity, as indicated by the direction of the arrows on the conductivity profiles in
516 Figure 7. Contrary to expectations, a noisy conductivity signal is always measured at high salinity, at
517 the beginning of the experiment, whereas equilibrated systems show a regular WII behavior at these
518 salinities. This phenomenon is due to a poor dispersion of droplets at the beginning of the
519 emulsification, due to the mild stirring and high interfacial tensions, which does not allow to get the
520 expected W/O emulsion. When the salinity approaches the optimal salinity range, the interfacial
521 tension falls, which favors the dispersion of droplets into the expected W/O emulsion morphology, as
522 indicated by the zero-conductivity signal. When salinity further decreases and reaches the optimal
523 salinity, the conductivity sharply increases at the phase inversion towards an O/W morphology.

524

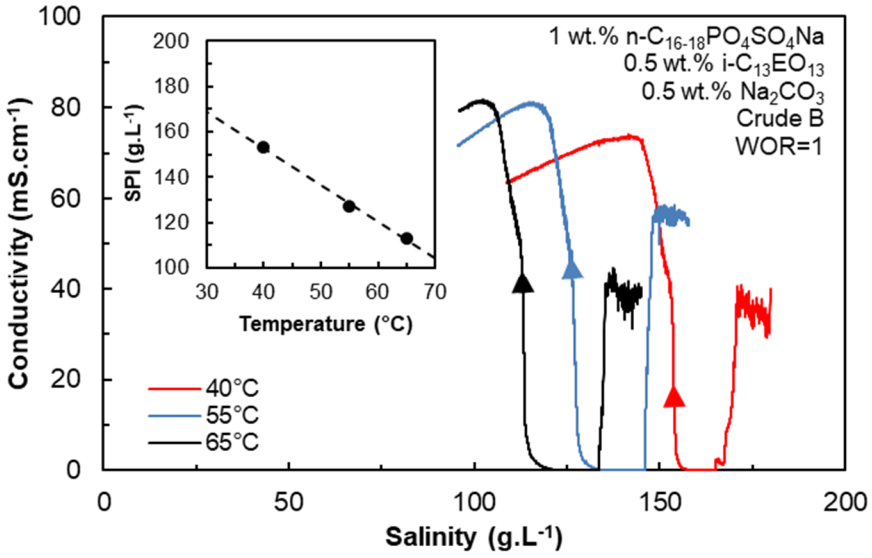

525

526 ***Figure 7**: Influence of temperature on the dynamic SPI of a petroleum SOW system (entries k-m of*

527 *Table 4)*

528 As the experiments were performed only by decreasing continuously the salinity, we could not

529 evidence hysteresis phenomena, but we can suspect they exist for this type of systems. As highlighted

530 in Figure 2 in Supplementary information, this hysteresis is more pronounced for crude oil-based

531 systems than for the model system 3 wt. % $C_{10}EO_4$/*n*-Octane/$NaCl_{(aq)}$ previously studied. However, it

532 does not impede the identification of the SPI even if the viscosity of the crude oil is quite high (176

533 mPa.s at 25°C). Figure 2 in SI also demonstrates that keeping a constant volume during the experiment

534 can increase the precision in the identification of the optimum formulation.

535

536 Figure 8 illustrates the impact of the concentration of nonionic co-surfactant for the *n*-$C_{16\text{-}18}PO_4SO_4Na$

537 1 % / *i*-$C_{10}EO_{10}$ x % with crude A without alkali (Table 4, entries b-d). Increasing the co-surfactant

538 concentration increases the global hydrophilicity of the surfactant system, as indicated by the higher

539 salinity required to attain the optimum formulation. A similar trend has already been reported by

540 *Salager et al.* who showed that increasing the amount of ethoxylated nonionic surfactant in a

541 nonionic/ionic mixture leads to an increase of optimum salinities [76]. For this system, the dynamic

542 SPI is linearly correlated with the amount of nonionic co-surfactant in the blend, as indicated by the

543 insert in Figure 8.

544 In this case also, it is interesting to look at the shapes of the conductivity profiles closely. Again, the
545 salinity has been continuously decreased to pass through the conditions of phase inversion. For the
546 system having the highest co-surfactant content (and therefore also the highest total surfactant
547 concentration), the expected W/O emulsion is obtained at high salinity at the beginning of the
548 experiment, as indicated by the zero-conductivity signal (violet curve in Figure 8). When the co-
549 surfactant content is reduced (green, red and blue curves), the same phenomenon as the one described
550 in Figure 8 is observed: the total amount of surfactant and/or the content of co-surfactant are not
551 enough to stabilize properly water droplets in oil at high salinity at the beginning of the experiment
552 (non-zero conductivity). When the salinity approaches the SPI, the oil/water interfacial tension is
553 reduced enough to favor the dispersion and a zero-conductivity is measured. The emulsion then reverts
554 to an O/W emulsion of high conductivity at the SPI. The range in which a W/O emulsion (zero-
555 conductivity signal) is obtained is very reduced for the system with 0.33% co-surfactant (red curve in
556 Figure 8), and even more for the system containing 0.25% co-surfactant (blue curve in Figure 8) which
557 do not form WIII systems at equilibrium (Table 2, entry o). For these concentrations, the shape of the
558 conductivity curves during the dynamic SPI gets close to what was observed in Figure 6, indicating a
559 very narrow area of low interfacial tensions (less than 3 $g.L^{-1}$). A non-inversion is observed when no
560 co-surfactant is added to the formulation (black curve in Figure 8).

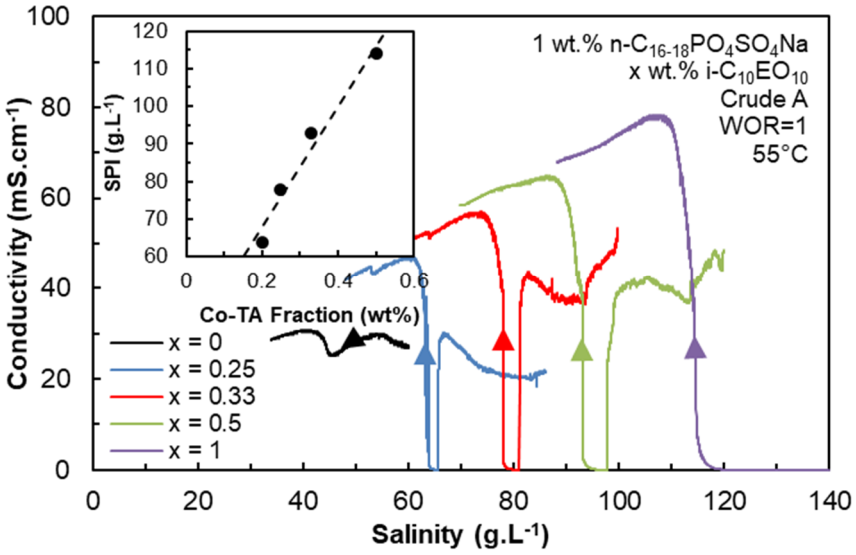

***Figure 8**: Influence of the nonionic co-surfactant concentration on the SPI of a petroleum SOW system (Table 4, entries b-d)*

3.3.5. Accuracy of the determination of optimal salinity by dynamic SPI

Finally, the data presented in Table 4 are represented graphically in Figure 9 to highlight the good correspondence between the dynamic SPI and the optimal salinity S* determined at equilibrium. A deviation lower than 10 % is observed. These data validate the dynamic SPI method as an alternative to the traditional static scans to find the conditions to reach the optimum formulation.

Its main advantage is a rapid execution - thirty minutes in average - coupled with a limited use of reactants. In the case of systems giving viscous phases instead of WIII microemulsions, a "SPI" is taken at the minimum of conductivity (see figure 6) and correlates with the salinity range in which gel phases are formed at equilibrium.

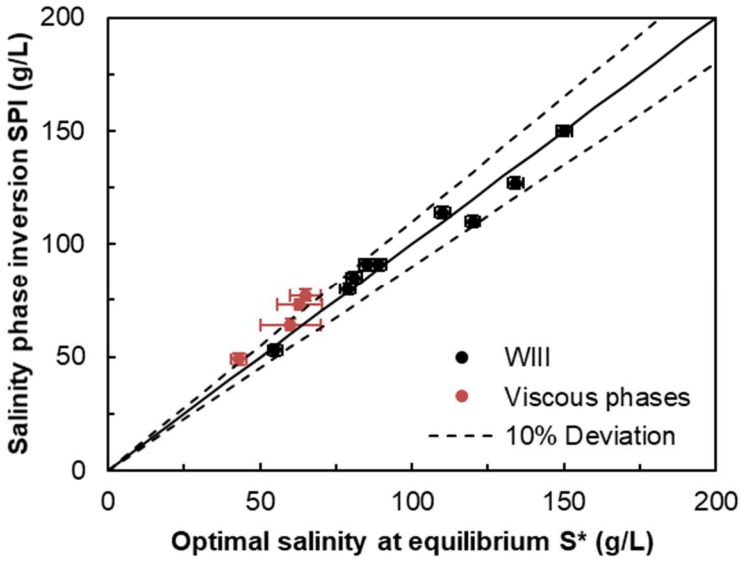

575

576 ***Figure 9****: Correlation between the dynamic salinity of phase inversion SPI and the optimal salinity*
577 *determined at equilibrium S* for the different petroleum-based SOW systems presented in Table 4. In*
578 *the case of non-inversion, the SPI is taken at the salinity of the negative spike (see Figure 6) and it is*
579 *related to the salinity range of formation of gel phases at equilibrium*

580

581 ## Conclusions

582 In this work, a new method to achieve a fast detection of the optimum formulation of Surfactant/Crude
583 oil/Brine at WOR in the vicinity of 1 is described. It is based on a continuous modification of the
584 salinity of a stirred and thermostated SOW system to cause a dynamic Salinity Phase Inversion (SPI)
585 of the emulsion detected by a sudden jump in conductivity. The study demonstrates that the phase
586 inversions of model and petroleum SOW systems are closely linked to their phase behavior at
587 equilibrium. The SPI experiment can be used to determine optimal salinities in a record time of thirty
588 minutes compared to equilibrium salinity scans carried out in the conventional manner. Moreover, the
589 shape of the conductivity curve was found to be a relevant descriptor for predicting and preventing the
590 formation of viscous phases generated when inappropriate surfactant blends are used with a given
591 crude oil.

For all these reasons, the dynamic SPI technique is particularly suitable for EOR applications and thanks to its fast implementation, it is particularly efficient for screening a large number of formulations in order to find rapidly the most effective surfactant systems. A variation of the technique is to trigger the phase inversion by continuously modifying the surfactant blend at a constant salinity. These dynamic experimental techniques can be carried out in conjunction with predictive models already described in the literature to accelerate even more the surfactant formulation screening [77–83].

More generally, this method has also a great potential for quantifying the sensitivity of surfactants to electrolytes. This will be described in a forthcoming paper. Finally, the SPI technique could be advantageously implemented to select the most efficient surface-active additives for other crude oil processing operations, such as wellbore cleaning, well injectivity restoration or demulsification.

Acknowledgments

The authors would like to thank TOTAL for financing G. Lemahieu PhD thesis and for allowing the publication of this work. BASF is also thanked for providing the surfactant samples.

We would also like to thank Maurice BOURREL and Nicolas PASSADE-BOUPAT for the helping discussions about petroleum phase behavior, EOR surfactant formulations and microemulsion correlations. We are also indebted to Corinne RICHARD for her valuable experimental contribution to this work.

Chevreul Institute (FR 2638), Ministère de l'Enseignement Supérieur et de la Recherche, Région Nord-Pas de Calais and FEDER are also acknowledged for supporting this work.

Conflict of interest

The authors declare that they have no conflict of interest.

References

[1] Boneau DF, Clampitt RL. A Surfactant System for the Oil-Wet Sandstone Of the North Burbank Unit. Journal of Petroleum Technology 1977;29:501–6. https://doi.org/10.2118/5820-PA.

[2] Healy RN, Reed RL. Immiscible Microemulsion Flooding. Society of Petroleum Engineers Journal 1977;17:129–39. https://doi.org/10.2118/5817-PA.

[3] Gogarty WB. Status of Surfactant or Micellar Methods. Journal of Petroleum Technology 1976;28:93–102. https://doi.org/10.2118/5559-PA.

[4] Schechter RS, Bourrel M. Microemulsions and related systems: formulation, solvency, and physical properties. M. Dekker; 1988.

[5] Bautista JF, Xu R, Fager A, Crouse B, Freed D. Improving Well Injectivity by Surfactant Flushing - A Digital Rock Study. SPE International Conference and Exhibition on Formation Damage Control, Lafayette, Louisiana, USA: Society of Petroleum Engineers; 2018. https://doi.org/10.2118/189549-MS.

[6] Pietrangeli G, Quintero L, Jones TA, Benaissa S, Menezes CA, Aubry E, et al. Overcoming Wellbore Cleanup Challenges in Deepwater Wells in West Africa. SPE International Symposium and Exhibition on Formation Damage Control, Lafayette, Louisiana, USA: Society of Petroleum Engineers; 2014. https://doi.org/10.2118/168215-MS.

[7] Bourrel M, Chambu C. The Rules for Achieving High Solubilization of Brine and Oil by Amphiphilic Molecules. Society of Petroleum Engineers Journal 1983;23:327–38. https://doi.org/10.2118/10676-PA.

[8] Nelson RC, Pope GA. Phase Relationships in Chemical Flooding. Society of Petroleum Engineers Journal 1978;18:325–38. https://doi.org/10.2118/6773-PA.

[9] Hirasaki G, Miller CA, Puerto M. Recent Advances in Surfactant EOR. SPE Journal 2011;16:889–907. https://doi.org/10.2118/115386-PA.

[10] Kamal MS, Hussein IA, Sultan AS. Review on Surfactant Flooding: Phase Behavior, Retention, IFT, and Field Applications. Energy Fuels 2017;31:7701–20. https://doi.org/10.1021/acs.energyfuels.7b00353.

[11] Bourrel M, Passade-Boupat N. Crude Oil Surface Active Species: Consequences for Enhanced Oil Recovery and Emulsion Stability. Energy Fuels 2018;32:2642–52. https://doi.org/10.1021/acs.energyfuels.7b02811.

[12] Barnes JR, Groen K, On A, Dubey ST, Reznik C, Buijse MA, et al. Controlled Hydrophobe Branching To Match Surfactant To Crude Composition For Chemical EOR. SPE Improved Oil Recovery Symposium, Tulsa, Oklahoma, USA: Society of Petroleum Engineers; 2012. https://doi.org/10.2118/154084-MS.

[13] Standard A. Standard test method for acid number of petroleum products by potentiometric titration-ASTM D 664-11A. ASTM International, West Conshohocken, PA 2011.

[14] D02 Committee. Test Method for Base Number of Petroleum Products by Potentiometric Perchloric Acid Titration. ASTM International; n.d. https://doi.org/10.1520/D2896-07.

[15] Passade-Boupat N, Zhou H, Rondon-Gonzalez M. Asphaltene Precipitation From Crude Oils : How To Predict It And To Anticipate Treatment? SPE Middle East Oil and Gas Show and Conference, Manama, Bahrain: Society of Petroleum Engineers; 2013. https://doi.org/10.2118/164184-MS.

[16] Fan T, Wang J, Buckley JS. Evaluating Crude Oils by SARA Analysis. SPE/DOE Improved Oil Recovery Symposium, Tulsa, Oklahoma: Society of Petroleum Engineers; 2002. https://doi.org/10.2118/75228-MS.

[17] Queste S, Salager JL, Strey R, Aubry JM. The EACN scale for oil classification revisited thanks to fish diagrams. Journal of Colloid and Interface Science 2007;312:98–107. https://doi.org/10.1016/j.jcis.2006.07.004.
[18] Huh C. Interfacial tensions and solubilizing ability of a microemulsion phase that coexists with oil and brine. Journal of Colloid and Interface Science 1979;71:408–26. https://doi.org/10.1016/0021-9797(79)90249-2.
[19] Huh C. Equilibrium of a Microemulsion That Coexists With Oil or Brine. Society of Petroleum Engineers Journal 1983;23:829–47. https://doi.org/10.2118/10728-PA.
[20] Sottmann T, Strey R. Ultralow interfacial tensions in water–n-alkane–surfactant systems. The Journal of Chemical Physics 1997;106:8606–15. https://doi.org/10.1063/1.473916.
[21] Princen HM, Zia IYZ, Mason SG. Measurement of interfacial tension from the shape of a rotating drop. Journal of Colloid and Interface Science 1967;23:99–107. https://doi.org/10.1016/0021-9797(67)90090-2.
[22] Salager J-L, Antón RE, Anderez JM, Aubry J-M. Formulation des micro-émulsions par la méthode HLD. Techniques de l'Ingénieur 2001;157:2001.
[23] Shinoda K, Arai H. The Correlation between Phase Inversion Temperature In Emulsion and Cloud Point in Solution of Nonionic Emulsifier. The Journal of Physical Chemistry 1964;68:3485–90. https://doi.org/10.1021/j100794a007.
[24] Shinoda K, Arai H. The effect of phase volume on the phase inversion temperature of emulsions stabilized with nonionic surfactants. Journal of Colloid and Interface Science 1967;25:429–31. https://doi.org/10.1016/0021-9797(67)90051-3.
[25] Salager JL, Loaiza-Maldonado I, Minana-Perez M, Silva F. Surfactant-oil-water systems near the affinity inversion Part I: Relationship between equilibrium phase behavior and emulsion type and stability. Journal of Dispersion Science and Technology 1982;3:279–92. https://doi.org/10.1080/01932698208943642.
[26] Salager JL, Miñana-Pérez M, Pérez-Sánchez M, Ramfrez-Gouveia M, Rojas CI. Surfactant-oil-water systems near the affinity inversion Part III: The two kinds of emulsion inversion. Journal of Dispersion Science and Technology 1983;4:313–29. https://doi.org/10.1080/01932698308943373.
[27] Pizzino A, Molinier V, Catté M, Ontiveros JF, Salager J-L, Aubry J-M. Relationship between Phase Behavior and Emulsion Inversion for a Well-Defined Surfactant ($C_{10}E_4$)/ *n* -Octane/Water Ternary System at Different Temperatures and Water/Oil Ratios. Industrial & Engineering Chemistry Research 2013;52:4527–38. https://doi.org/10.1021/ie302772u.
[28] Smith DH, Lim K-H. A Study of the Morphologies and Inversions of Model Oilfield Dispersions. SPE Production Engineering 1990;5:265–9. https://doi.org/10.2118/18496-PA.
[29] Lira K-H, Smith DH. Electrical conductivities of concentrated emulsions and their fit by conductivity models. Journal of Dispersion Science and Technology 1990;11:529–45. https://doi.org/10.1080/01932699008943276.
[30] Charin RM, Araújo BC, Farias AC, Tavares FW, Nele M. Studies on transitional emulsion phase inversion using the steady state protocol. Colloids and Surfaces A: Physicochemical and Engineering Aspects 2015;484:424–33. https://doi.org/10.1016/j.colsurfa.2015.08.003.
[31] Ontiveros JF, Pierlot C, Catté M, Molinier V, Salager J-L, Aubry J-M. Structure–interfacial properties relationship and quantification of the amphiphilicity of well-defined ionic and non-ionic surfactants using the PIT-slope method. Journal of Colloid and Interface Science 2015;448:222–30. https://doi.org/10.1016/j.jcis.2015.02.028.
[32] Ontiveros JF, Pierlot C, Catté M, Molinier V, Salager J-L, Aubry J-M. A simple method to assess the hydrophilic lipophilic balance of food and cosmetic surfactants using the phase inversion temperature of C10E4/n-octane/water emulsions. Colloids and Surfaces A: Physicochemical and Engineering Aspects 2014;458:32–9. https://doi.org/10.1016/j.colsurfa.2014.02.058.
[33] Ontiveros JF, Pierlot C, Catté M, Salager J-L, Aubry J-M. Determining the Preferred Alkane Carbon Number (PACN) of nonionic surfactants using the PIT-slope method. Colloids and Surfaces A:

716 Physicochemical and Engineering Aspects 2018;536:30–7.
717 https://doi.org/10.1016/j.colsurfa.2017.08.002.
718 [34] Lemahieu G, Ontiveros JF, Molinier V, Aubry J-M. Using the dynamic Phase Inversion
719 Temperature (PIT) as a fast and effective method to track optimum formulation for Enhanced Oil
720 Recovery. Journal of Colloid and Interface Science 2019;557:746–56.
721 https://doi.org/10.1016/j.jcis.2019.09.050.
722 [35] Pierlot C, Ontiveros JF, Catté M, Salager J-L, Aubry J-M. Cone–Plate Rheometer as Reactor and
723 Viscosity Probe for the Detection of Transitional Phase Inversion of Brij30–Isopropyl Myristate–
724 Water Model Emulsion. Industrial & Engineering Chemistry Research 2016;55:3990–9.
725 https://doi.org/10.1021/acs.iecr.6b00399.
726 [36] Salager JL, Mi∼ana-Pérez M, Andérez JM, Grosso JL, Rojas CI, Layrisse I, et al. Surfactant-oil-
727 water systems near the affinity inversion part II: Viscosity of emulsified systems. Journal of
728 Dispersion Science and Technology 1983;4:161–73.
729 https://doi.org/10.1080/01932698308943361.
730 [37] Allouche J, Tyrode E, Sadtler V, Choplin L, Salager J-L. Simultaneous Conductivity and Viscosity
731 Measurements as a Technique To Track Emulsion Inversion by the Phase-Inversion-Temperature
732 Method. Langmuir 2004;20:2134–40. https://doi.org/10.1021/la035334r.
733 [38] Tolosa L-I, Forgiarini A, Moreno P, Salager J-L. Combined Effects of Formulation and Stirring on
734 Emulsion Drop Size in the Vicinity of Three-Phase Behavior of Surfactant−Oil Water Systems.
735 Industrial & Engineering Chemistry Research 2006;45:3810–4.
736 https://doi.org/10.1021/ie060102j.
737 [39] Charin RM, Nele M, Tavares FW. Transitional Phase Inversion of Emulsions Monitored by in Situ
738 Near-Infrared Spectroscopy. Langmuir 2013;29:5995–6003. https://doi.org/10.1021/la4007263.
739 [40] de Oliveira Honse S, Kashefi K, Charin RM, Tavares FW, Pinto JC, Nele M. Emulsion phase
740 inversion of model and crude oil systems detected by near-infrared spectroscopy and principal
741 component analysis. Colloids and Surfaces A: Physicochemical and Engineering Aspects
742 2018;538:565–73. https://doi.org/10.1016/j.colsurfa.2017.11.028.
743 [41] Pizzino A, Rodriguez MP, Xuereb C, Catté M, Van Hecke E, Aubry J-M, et al. Light Backscattering
744 as an Indirect Method for Detecting Emulsion Inversion. Langmuir 2007;23:5286–8.
745 https://doi.org/10.1021/la070090m.
746 [42] Pizzino A, Catté M, Van Hecke E, Salager J-L, Aubry J-M. On-line light backscattering tracking of
747 the transitional phase inversion of emulsions. Colloids and Surfaces A: Physicochemical and
748 Engineering Aspects 2009;338:148–54. https://doi.org/10.1016/j.colsurfa.2008.05.041.
749 [43] Shinoda K, Saito H. The Stability of O/W type emulsions as functions of temperature and the HLB
750 of emulsifiers: The emulsification by PIT-method. Journal of Colloid and Interface Science
751 1969;30:258–63. https://doi.org/10.1016/S0021-9797(69)80012-3.
752 [44] Shinoda K, Takeda H. The effect of added salts in water on the hydrophile-lipophile balance of
753 nonionic surfactants: The effect of added salts on the phase inversion temperature of emulsions.
754 Journal of Colloid and Interface Science 1970;32:642–6. https://doi.org/10.1016/0021-
755 9797(70)90157-8.
756 [45] Shinoda K, Kunieda H. Conditions to produce so-called microemulsions: Factors to increase the
757 mutual solubility of oil and water by solubilizer. Journal of Colloid and Interface Science
758 1973;42:381–7. https://doi.org/10.1016/0021-9797(73)90303-2.
759 [46] Salager JL, Quintero L, Ramos E, Anderez J. Properties of surfactant/oil/water emulsified systems
760 in the neighborhood of the three-phase transition. Journal of Colloid and Interface Science
761 1980;77:288–9. https://doi.org/10.1016/0021-9797(80)90447-6.
762 [47] Scriven LE. Equilibrium bicontinuous structure. Nature 1976;263:123–5.
763 https://doi.org/10.1038/263123a0.
764 [48] Chan KS, Shah DO. The Effect Of Surfactant Partitioning On The Phase Behavior And Phase
765 Inversion Of The Middle Phase Microemulsions. SPE Oilfield and Geothermal Chemistry
766 Symposium, Houston, Texas: Society of Petroleum Engineers; 1979.
767 https://doi.org/10.2118/7869-MS.

[49] Kunz W, Testard F, Zemb T. Correspondence between Curvature, Packing Parameter, and Hydrophilic−Lipophilic Deviation Scales around the Phase-Inversion Temperature. Langmuir 2009;25:112–5. https://doi.org/10.1021/la8028879.
[50] Lemahieu G, Ontiveros JF, Molinier V, Aubry J. Revisiting the Phase Inversion Temperature as a Practical Tool for EOR Applications, IOR 2019 – 20th European Symposium on Improved Oil Recovery, Pau, France: 2019. https://doi.org/10.3997/2214-4609.201900166.
[51] Kunieda H, Yamagata M. Mixing of nonionic surfactants at water-oil interfaces in microemulsions. Langmuir 1993;9:3345–51. https://doi.org/10.1021/la00036a005.
[52] Antón RE, Castillo P, Salager JL. Surfactant-oil-water systems near the affinity inversion part IV: emulsion inversion temperature. Journal of Dispersion Science and Technology 1986;7:319–29. https://doi.org/10.1080/01932698608943463.
[53] Antón R, Rivas H, Salager J-L. Surfactant-oil-water systems near the affinity inversion. part x: emulsions made with anionic-nonionic surfactant mixtures. Journal of Dispersion Science and Technology 1996;17:553–66. https://doi.org/10.1080/01932699608943524.
[54] Márquez L, Graciaa A, Lachaise J, Salager J-L, Zambrano N. Hysteresis behaviour in temperature-induced emulsion inversion: Hysteresis in temperature-induced emulsion inversion. Polym Int 2003;52:590–3. https://doi.org/10.1002/pi.1046.
[55] Aubry J-M, Ontiveros JF, Salager J-L, Nardello-Rataj V. Use of the normalized hydrophilic-lipophilic-deviation (HLDN) equation for determining the equivalent alkane carbon number (EACN) of oils and the preferred alkane carbon number (PACN) of nonionic surfactants by the fish-tail method (FTM). Advances in Colloid and Interface Science 2020;276:102099. https://doi.org/10.1016/j.cis.2019.102099.
[56] Witthayapanyanon A, Harwell JH, Sabatini DA. Hydrophilic–lipophilic deviation (HLD) method for characterizing conventional and extended surfactants. Journal of Colloid and Interface Science 2008;325:259–66. https://doi.org/10.1016/j.jcis.2008.05.061.
[57] Kahlweit M, Strey R, Schomaecker R, Haase D. General patterns of the phase behavior of mixtures of water, nonpolar solvents, amphiphiles, and electrolytes. 2. Langmuir 1989;5:305–15. https://doi.org/10.1021/la00086a002.
[58] Graciaa A, Lachaise J, Sayous JG, Grenier P, Yiv S, Schechter RS, et al. The partitioning of complex surfactant mixtures between oil/water/microemulsion phases at high surfactant concentrations. Journal of Colloid and Interface Science 1983;93:474–86. https://doi.org/10.1016/0021-9797(83)90431-9.
[59] Sager WFC. Systematic Study on the Influence of Impurities on the Phase Behavior of Sodium Bis(2-ethylhexyl) Sulfosuccinate Microemulsions. Langmuir 1998;14:6385–95. https://doi.org/10.1021/la9709608.
[60] Rosen MJ, Kunjappu JT. Surfactants and interfacial phenomena. 4th ed. Hoboken, N.J: Wiley; 2012.
[61] Salager J-L, Forgiarini AM, Bullón J. How to Attain Ultralow Interfacial Tension and Three-Phase Behavior with Surfactant Formulation for Enhanced Oil Recovery: A Review. Part 1. Optimum Formulation for Simple Surfactant–Oil–Water Ternary Systems. Journal of Surfactants and Detergents 2013;16:449–72. https://doi.org/10.1007/s11743-013-1470-4.
[62] Healy RN, Reed RL, Stenmark DG. Multiphase Microemulsion Systems. Society of Petroleum Engineers Journal 1976;16:147–60. https://doi.org/10.2118/5565-PA.
[63] Verkruyse LA, Salter SJ. Potential Use of Nonionic Surfactants in Micellar Flooding. SPE Oilfield and Geothermal Chemistry Symposium, Phoenix, Arizona: Society of Petroleum Engineers; 1985. https://doi.org/10.2118/13574-MS.
[64] Graciaa A, Fortney LN, Schechter RS, Wade WH, Yiv S. Criteria for Structuring Surfactants To Maximize Solubilization of Oil and Water: Part 1-Commercial Nonionics. Society of Petroleum Engineers Journal 1982;22:743–9. https://doi.org/10.2118/9815-PA.
[65] Barakat Y, Fortney LN, Schechter RS, Wade WH, Yiv SH, Graciaa A. Criteria for structuring surfactants to maximize solubilization of oil and water. Journal of Colloid and Interface Science 1983;92:561–74. https://doi.org/10.1016/0021-9797(83)90177-7.

[66] Salager J-L, Forgiarini AM, Márquez L, Manchego L, Bullón J. How to Attain an Ultralow Interfacial Tension and a Three-Phase Behavior with a Surfactant Formulation for Enhanced Oil Recovery: A Review. Part 2. Performance Improvement Trends from Winsor's Premise to Currently Proposed Inter- and Intra-Molecular Mixtures. Journal of Surfactants and Detergents 2013;16:631–63. https://doi.org/10.1007/s11743-013-1485-x.
[67] Wade WH, Morgan JC, Schechter RS, Jacobson JK, Salager JL. Interfacial Tension and Phase Behavior of Surfactant Systems. Society of Petroleum Engineers Journal 1978;18:242–52. https://doi.org/10.2118/6844-PA.
[68] Binks BP, Meunier J, Abillon O, Langevin D. Measurement of film rigidity and interfacial tensions in several ionic surfactant-oil-water microemulsion systems. Langmuir 1989;5:415–21. https://doi.org/10.1021/la00086a022.
[69] Bourrel M, Koukounis Ch, Schechter R, Wade W. Phase and interfacial tension behavior of nonionic surfactants. Journal of Dispersion Science and Technology 1980;1:13–35. https://doi.org/10.1080/01932698008962159.
[70] Zhao P, Jackson A, Britton C, Kim DH, Britton LN, Levitt D, et al. Development of High-Performance Surfactants for Difficult Oils. SPE Symposium on Improved Oil Recovery, Tulsa, Oklahoma, USA: Society of Petroleum Engineers; 2008. https://doi.org/10.2118/113432-MS.
[71] Levitt D, Jackson A, Heinson C, Britton LN, Malik T, Dwarakanath V, et al. Identification and Evaluation of High-Performance EOR Surfactants. SPE/DOE Symposium on Improved Oil Recovery, Tulsa, Oklahoma, USA: Society of Petroleum Engineers; 2006. https://doi.org/10.2118/100089-MS.
[72] Tagavifar M, Fortenberry R, de Rouffignac E, Sepehrnoori K, Pope GA. Heavy-Oil Recovery by Combined Hot Water and Alkali/Cosolvent/Polymer Flooding. SPE Journal 2016;21:074–86. https://doi.org/10.2118/170161-PA.
[73] Molinier V, Klimenko A, Loriau M, Ligiero L, Bourrel M, Passade-Boupat N. Isolation and Characterization of Endogenous Crude Oil Surface Active Species and their Implication in the Formulation of Surfactants for EOR, Pau, France: 2019. https://doi.org/10.3997/2214-4609.201900111.
[74] Kiran SK, Acosta EJ, Moran K. Evaluating the hydrophilic–lipophilic nature of asphaltenic oils and naphthenic amphiphiles using microemulsion models. Journal of Colloid and Interface Science 2009;336:304–13. https://doi.org/10.1016/j.jcis.2009.03.053.
[75] Hammond CE, Acosta EJ. On the Characteristic Curvature of Alkyl-Polypropylene Oxide Sulfate Extended Surfactants. Journal of Surfactants and Detergents 2012;15:157–65. https://doi.org/10.1007/s11743-011-1303-2.
[76] Salager J-L, Forgiarini AM, Rondón MJ. How to Attain Ultralow Interfacial Tension and Three-Phase Behavior with a Surfactant Formulation for Enhanced Oil Recovery: a Review—Part 3. Practical Procedures to Optimize the Laboratory Research According to the Current State of the Art in Surfactant Mixing. J Surfact Deterg 2017;20:3–19. https://doi.org/10.1007/s11743-016-1883-y.
[77] Buijse MA, Tandon K, Jain S, Handgraaf J-W, Fraaije J. Surfactant Optimization for EOR using Advanced Chemical Computational Methods. SPE Improved Oil Recovery Symposium, Tulsa, Oklahoma, USA: Society of Petroleum Engineers; 2012. https://doi.org/10.2118/154212-MS.
[78] Solairaj S, Britton C, Lu J, Kim DH, Weerasooriya U, Pope GA. New Correlation to Predict the Optimum Surfactant Structure for EOR. SPE Improved Oil Recovery Symposium, Tulsa, Oklahoma, USA: Society of Petroleum Engineers; 2012. https://doi.org/10.2118/154262-MS.
[79] Fraaije JGEM, Tandon K, Jain S, Handgraaf J-W, Buijse M. Method of Moments for Computational Microemulsion Analysis and Prediction in Tertiary Oil Recovery. Langmuir 2013;29:2136–51. https://doi.org/10.1021/la304505u.
[80] Buijse MA, Tandon K, Jain S, Jain A, Handgraaf J-W, Fraaije JGEM. Accelerated Surfactant Selection for EOR Using Computational Methods. SPE Enhanced Oil Recovery Conference, Kuala Lumpur, Malaysia: Society of Petroleum Engineers; 2013. https://doi.org/10.2118/165268-MS.

[81] Jin L, Jamili A, Li Z, Lu J, Luo H, Ben Shiau BJ, et al. Physics based HLD–NAC phase behavior model for surfactant/crude oil/brine systems. Journal of Petroleum Science and Engineering 2015;136:68–77. https://doi.org/10.1016/j.petrol.2015.10.039.
[82] Ghosh S, Johns RT. Dimensionless Equation of State to Predict Microemulsion Phase Behavior. Langmuir 2016;32:8969–79. https://doi.org/10.1021/acs.langmuir.6b02666.
[83] Ghosh S, Johns RT. An Equation-of-State Model To Predict Surfactant/Oil/Brine-Phase Behavior. SPE Journal 2016;21:1106–25. https://doi.org/10.2118/170927-PA.

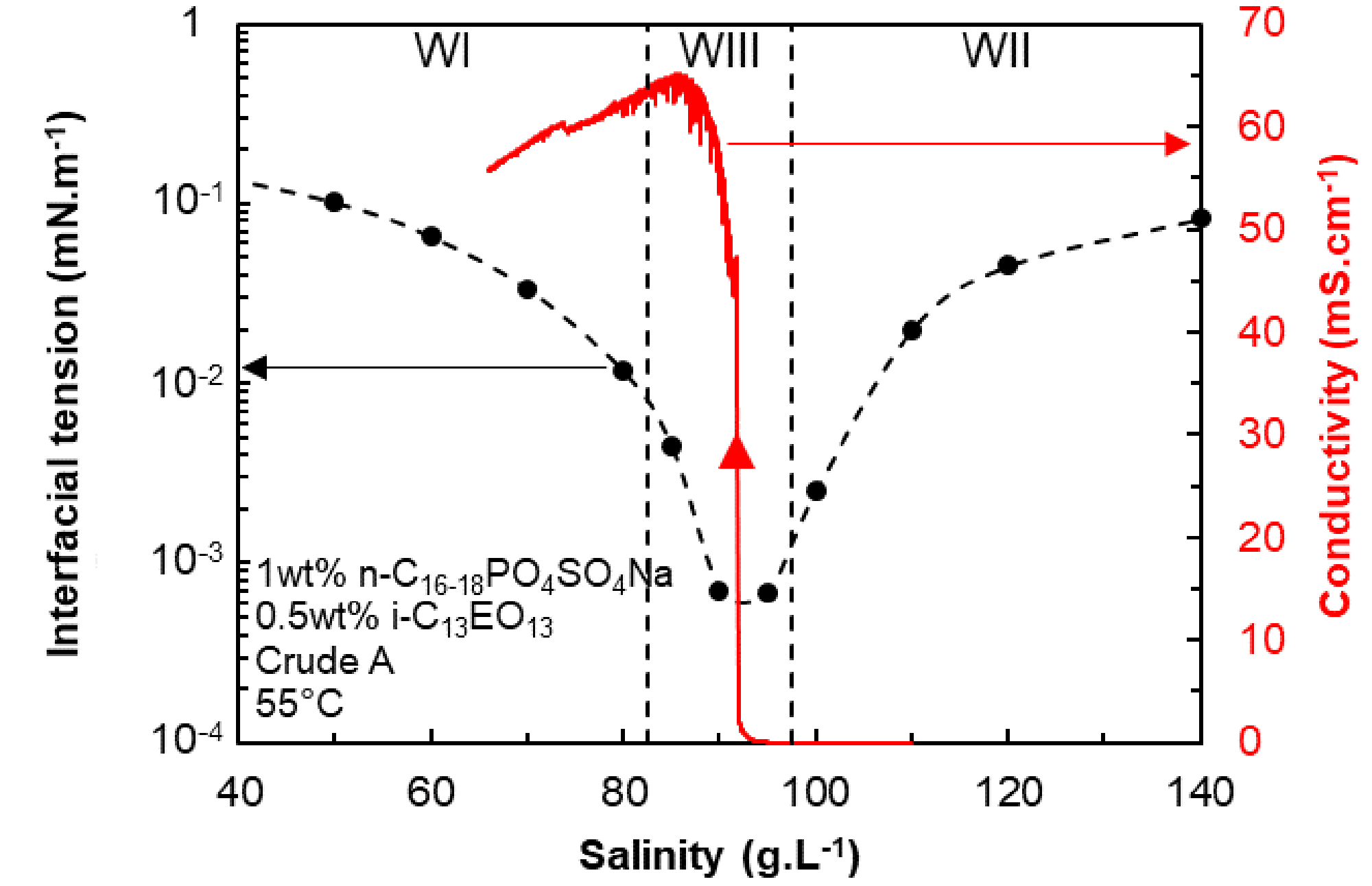
WI
WIII
WII
1
10^{-1}
10^{-2}
10^{-3}
10^{-4}
Interfacial tension (mN.m^{-1})
70
60
50
40
30
20
10
0
Conductivity (mS.cm^{-1})
1wt% n-$C_{16-18}PO_4SO_4Na$
0.5wt% i-$C_{13}EO_{13}$
Crude A
55°C
40
60
80
100
120
140
Salinity (g.L^{-1})